International Journal of Mining Science and Technology 26 (2016) 487–494

Contents lists available at ScienceDirect

International Journal of Mining Science and Technology

journal homepage: www.elsevier.com/locate/ijmst

# DPM simulation in an underground entry: Comparison between particle and species models

Thiruvengadam Magesh [a,*], Zheng Yi [a], Tien Jerry C. [b]

[a] Department of Mining & Nuclear Engineering, Missouri University of Science & Technology, Rolla, MO 65401, USA
[b] Division of Mining and Resources Engineering, Department of Civil Engineering, Monash University, VIC 3800, Australia

ARTICLE INFO

*Article history:*
Received 4 June 2015
Received in revised form 11 September 2015
Accepted 13 January 2016
Available online 15 March 2016

*Keywords:*
CFD
Dead-end
DPM
Discrete phase model
Species transport model

ABSTRACT

The diesel particulate matter (DPM) emission from diesel powered equipment in underground mines can cause health hazards including cancer to the miners. The understanding of the DPM propagation pattern under realistic mining condition is required for selecting proper DPM control strategies and to improve working practices in underground mines. In this paper, three dimensional simulations of DPM emission from the exhaust tail pipe of a load-haul-dump (LHD) vehicle and its subsequent distribution inside an isolated zone in the typical underground mine are carried out using two different solution models available in Ansys Fluent. The incoming fresh air into the isolated zone is treated as a continuous phase and DPM is treated either as a continuous phase (gas) or as a secondary discrete phase (particle). Species transport model is used when DPM is treated as gas and discrete phase model is used when DPM is assumed to behave like a particle. The distributions of DPM concentration inside the isolated zone obtained from each method are presented and compared. From the comparison results, an accurate and economical solution technique for DPM evaluation can be selected.



## 1. Introduction

Diesel engine operated LHDs and trucks are widely used in underground metal/non-metal mines. Although they have better fuel efficiency, emission from the tail pipe and its subsequent distribution in the underground mine are of growing concern for miners. DPM is the particulate byproduct of diesel exhaust and it can exist in different modes with different size distributions (5 nm–10 μm). 90% of the DPM emitted from the diesel engines have size distributions in nanometer ranges. Due to its very small size, it will remain airborne for long duration of time and pollutes the entire mine environment causing health hazard to the miners. It is established that long time exposure to diesel exhaust can lead to cancer, asthma and other health effects such as eye and nose irritation, headaches and nausea [1–6].

Many researchers have carried out both experimental and numerical studies on diesel particle matter emission. For example, Kim et al. studied formation of DPM inside the turbulent exhaust plume of a diesel vehicle [7]. They used Ansys Fluent computational fluid dynamics (CFD) code to determine the formation of diesel particulates by nucleation and coagulation. Uhrner et al. studied the turbulent diffusion of plume exhaust from the diesel engine using both experimental and numerical approach [8]. Another interesting study on the deposition of ultra-fine particles from diesel exhaust aerosol was carried by Desantes et al. [9]. Henrik Strom and Bengt Andersson performed Eulerian–Lagrangian CFD modeling to simulate trapping of diesel and gasoline particulate matter in flow-through devices [10]. They used eight different types of diesel and gasoline particulate matter (different densities) in their simulation. Although all these studies are related to the diesel particulate matter, these are not related to the mine environment.

In the underground environment, Ray et al. studied $NO_2$ distribution for underground passenger railroad tunnel utilizing diesel locomotives [11]. CFD was used to evaluate the effectiveness of natural and mechanical ventilation system. Simulation of DPM dispersion in underground metal/nonmetal mines was carried out by Zheng and Tien [12]. In this study, the DPM was considered to behave like a gas and not as particle. The treatment of DPM as a gas was later incorporated the buoyancy effect and compared with a test, in which the simulation agreed with the test at a practical accuracy [13,14]. Kurnia et al. studied a diesel powered continuous miner and shuttle car face with CFD to simulate the distribution of hazardous gases and optimize the local ventilation system [15].

In other mining studies, CFD simulations have been used in mining research to detect spontaneous combustion and apply

* Corresponding author. Tel.: +1 573 3417688.
*E-mail address:* mtwv8@mst.edu (M. Thiruvengadam).

http://dx.doi.org/10.1016/j.ijmst.2016.02.018
2095-2686/

inertization in gob areas, study airflow patterns and gas concentrations in continuous miner face ventilation configurations, investigate scrubber intake designs and water mist flow for longwall dust control, and estimate a mine's ventilation status after a disaster [16–25].

The present study focuses on the diesel particulate emission and its diffusion inside the underground mine areas. To the author's knowledge, the study of DPM inside the underground metal/non-metal mines assuming DPM to behave like a particle than as a gas was not considered and that motivated the present study. In this paper, a region of an isolated zone at Noranda Inc.-Brunswick Mine was selected to conduct a CFD study to determine the DPM distribution pattern and to identify locations with high DPM concentration [26]. The CFD study was conducted using both discrete phase model and species transport model available in Fluent. The comparison between these models is made and the results are presented in this study.

## 2. Diesel emission evaluation program (DEEP)

The objective of the DEEP field study conducted in an isolated zone at Noranda Brunswick Mine was to investigate the effectiveness of the diesel particulate filter (DPF) in the underground mine environment [26]. They selected LHD vehicles and haulage trucks fitted with DPF filters to do the study. The section of drift is about 400 m long and the vehicles were operated inside this 400 m zone by repeating an 8 min production cycle. The layout for this isolated zone along with the locations of the three DPM sampling stations is shown in Fig. 1. From this study, the average carbon concentration at the exhaust sampling station were obtained for different vehicles and the results are shown in Fig. 2. The configuration of this isolated zone along with the measured results from this study will be used in the present CFD analysis to predict the DPM distribution and to identify the regions that exceeds the current regulatory requirement for DPM concentration (>160 μg/m$^3$) in this isolated zone.

## 3. Problem statement

A portion of the isolated zone shown in Fig. 1 (approximately 134 m) with one dead-end is selected for the present computational study. An LHD vehicle is placed inside this single entry with its tail pipe emission against the direction as that of the fresh air flow. Three-dimensional turbulent simulation of diesel particulate matter is carried out and a schematic of the computational domain is shown in Fig. 3. The length of the single entry ($L$) measures approximately 134 m. The height ($H$) and width ($W$) are 4.8 and 4.0 m respectively at the inlet. The physical properties of fresh air flow are treated as constants and evaluated for inlet temperature of $T_0$ = 27 °C (i.e., specific heat ($C_p$) is 1006 J/(kg K), dynamic viscosity ($\mu$) is $1.789 \times 10^{-5}$ kg/(m s), and thermal conductivity ($k$) equals to 0.0242 W/(m K)).

The density variation in the fluid due to temperature gradient that exists between the air intake temperature and the tailpipe

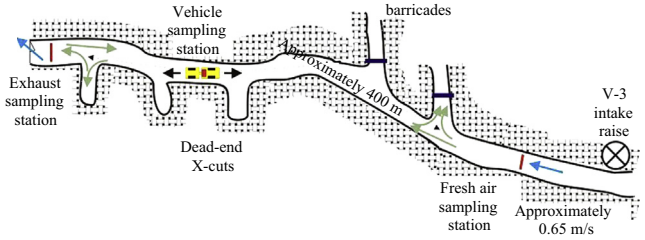


**Fig. 1.** Isolated zone layout in DEEP field study [26].

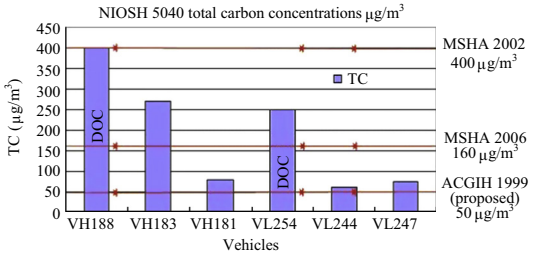


**Fig. 2.** Total carbon concentrations at the exhaust sampling station [26].

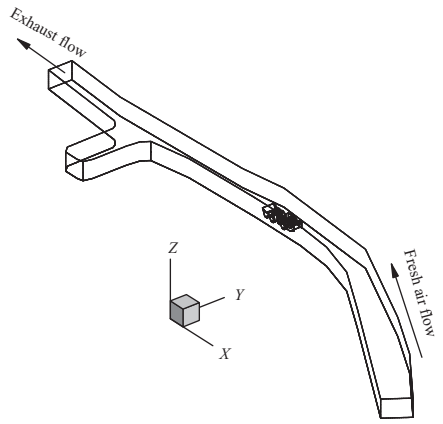


**Fig. 3.** Schematic of the single entry with one dead-end.

emission temperature is calculated using the incompressible ideal gas model available in Fluent. In this model, the flow is assumed to be incompressible but density change due to temperature is calculated using ideal gas law. In the presence of gravity, this density gradient results in buoyancy flow. Numerical simulation of DPM distribution inside the single entry is performed using the discrete phase model and species transport model available in Fluent.

In the discrete phase model, particles are assumed to be of inert type and having constant diameter $d_p$ = 70 nm. The physical properties of the particle are treated as constants with density ($\rho_d$ = 1000 kg/m$^3$), specific heat ($C_p$ = 1220 J/(kg K)) and thermal conductivity ($k$ = 0.0242 W/(m K)). The thermal conductivity of particles is assumed to be equal to that of air (i.e. $k_p = k_{air}$). This is due to the reduced heat conductivity of nano-sized particles [27]. In the present study, two-way coupling (the interaction of the gas phase with particles and vice versa) is considered. So the particles can exchange heat and momentum with continuous phase (air). The limitation in this model is that particle–particle interaction is neglected. The DPM from the tail pipe of LHD is injected into the simulation domain using surface injection option available in discrete phase model of Fluent. The DPM is injected into the computational domain for every fluid flow (continuous phase) time step. The tailpipe boundary surface is made up of 44 cell faces. In surface injection, one particle packet is released from each cell face and overall 44 particle packets from the tailpipe surface for each time step. Each particle packet will contain millions of individual particles and the discrete phase tracks the particle packets rather than millions of individual particles since it is practically impossible to track them computationally [28]. The number of individual particles in each packet will vary depending on the time step used to satisfy the DPM mass flow rate requirements.

In the species transport model, DPM is treated as gas (continuous phase) and the material that is selected as a representative for the DPM is $n$-octane vapor ($C_8H_{18}$) with density ($\rho$ = 4.84 kg/m$^3$),

specific heat ($C_p$ = 2467 J/(kg K)), thermal conductivity ($k$ = 0.0178 W/(m K)) and dynamic viscosity ($\mu = 6.75 \times 10^{-5}$ kg/(m s)). In the species transport model, the two species air and DPM can diffuse and form a mixture. The mixture properties are derived using incompressible ideal gas law for density, mixing law for specific heat, thermal conductivity and viscosity. The mass diffusivity between air and DPM is assumed to be constant with $D = 5 \times 10^{-6}$ m$^2$/s. The chemical reaction between the species is not considered in this study.

## 4. Governing equations and boundary conditions

The air flow inside the computational domain is solved in Eulerian frame as continuous phase using time averaged three-dimensional transient Navier–Stokes, energy, and continuity equations using the finite volume method. In the species transport model, an additional non reacting two species transport equation (DPM and Air) is solved in Eulerian reference frame (since both air and DPM are treated as continuous phase) to determine the mass fraction of DPM. In the discrete phase model, the DPM is tracked inside the continuous phase (air) using particle tracking method (discrete phase model) of Fluent in Lagrangian frame.

The important forces acting on the particle are the drag force, lift force and the gravity force (buoyancy force). The particle trajectory inside the gas phase is determined by integrating the particle force balance equation written in Lagrangian reference frame in the $i$ direction as [28].

$$\frac{du_i^p}{dt} = F_D(u_i - u_i^p) + g_i(\rho_p - \rho)/\rho_p + F_i \quad (1)$$

where $u_i$ is the fluid phase velocity; $u_i^p$ the particle velocity; $\rho$ the fluid density; and $\rho_p$ the particle density. The term $F_D(u_i - u_i^p)$ is the drag force per unit particle mass and $F_D$ given by Stokes-Cunningham drag law,

$$F_D = \frac{18\mu}{\rho_P d_P^2 C_C} \quad (2)$$

where $C_C = 1 + 2\lambda/d_P(1.257 + 0.4e^{-(1.1d_P/2\lambda)})$ is the Cunningham correction factor for sub-micron particles. Here $\lambda = 6.6 \times 10^{-8}$ m is the mean free path of the molecules of air. The second term on the right hand side of Eq. (1) is the gravity force and the last term $F_i$ includes all the additional forces that are acting on the particle, namely lift force, thermophoretic force, Brownian force and pressure gradient force. The lift force is modeled using Saffman's lift force equation.

From the dimensions at the inlet, the hydraulic diameter ($D = 4A/P$) (here $A$ is the inlet cross-sectional area and $P$ the perimeter), is calculated as $D$ = 4.38 m. The Reynolds number calculated based on this hydraulic diameter ($D$) is $Re = 2 \times 10^5$ and the flow at this Reynolds number is turbulent. The turbulence in the flow is modeled using standard $k$–$\varepsilon$ turbulence model with standard wall functions for near wall treatment for both particle tracking and species transport model. The dispersion of particles due to turbulence in the air is predicted using a stochastic tracking model to include the effect of turbulent velocity fluctuations on the particle trajectories. Table 1 shows boundary conditions used to determine the DPM distribution inside the single entry.

**Table 1**
Boundary conditions used for DPM simulation.

| Boundary | Boundary condition |
|---|---|
| Air inlet | Velocity (normal to boundary) = 0.65 m/s, $T$ = 300 K, DPM mass fraction = 0 (DPM as gas) |
| Exit | Outflow or fully developed boundary conditions |
| LHD-tailpipe | $U$ = 24.1 m/s, $V$ = 0 m/s and $W$ = 0 m/s; $T$=594 K<br>DPM as particle (assign DPM injection conditions)<br>$U$ = 24.1 m/s, $V$ = 0 m/s and $W$ = 0 m/s<br>$T$ = 594 K; mass flow rate: 7.2e−07 kg/s; particle diameter: ($d_p$) = 70 nm<br>DPM as gas (assign DPM mass fraction)<br>DPM ($C_8H_{18}$) mass fraction = 1.73e−06 [29,30] |
| Wall | No slip boundary conditions and adiabatic walls |

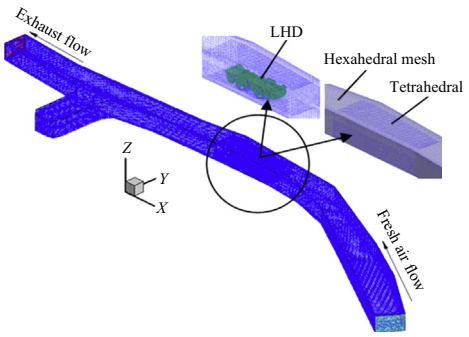


**Fig. 4.** Mesh inside the computational domain.

## 5. Mesh generation and solution procedure

The computational domain is meshed using Gambit as shown in Fig. 4. In order to ensure the accuracy of the simulation, the mesh generation is made by ensuring high density near the truck and in the bounding wall regions where high gradients exist. Both hexahedral and tetrahedral meshes were generated inside the computational domain as shown in Fig. 4. During mesh generation, the equi-size skew is monitored and maintained at a value less than 0.8.

Numerical solution of the governing equations and boundary conditions are performed by utilizing the commercial CFD code Ansys Fluent 12.0. The SIMPLE algorithm is used for the pressure velocity coupling. In order to improve the accuracy of simulations, the momentum, scalar turbulence, energy and species transport equations are discretized using the second order upwind scheme. Second order discretization scheme is used for the pressure equation. Least square cell based method is used to compute gradients in the governing equations. Detailed descriptions of the CFD code and the solution procedures may be found in the Ansys Fluent 12.0 documentation [28]. The unsteady flow calculations are made using time step ($\Delta t$ = 0.01 s) for the time period of 200 s for both species and discrete phase model. The convergence criterion required that the scaled residuals be smaller than $10^{-4}$ for the mass, momentum, turbulent and species transport equations and smaller than $10^{-9}$ for the energy equation. Calculations were performed on Nic Cluster using 16 processors; and the CPU time for converged solution for particle tracking method was approximately 48 h in order to obtain results for 200 s. The CPU time required for species transport model for the same time period is only about one-half of that required for particle tracking method. This difference is because of the large storage space requirement for storing particle tracking information when DPM is treated as particle.

## 6. Results and discussion

Unsteady simulations are carried out to predict DPM distributions in the single entry that is presented in Fig. 3 using Fluent CFD code. All the results that are discussed in this section are for the case (1) designed inlet fresh air velocity of 0.65 m/s and (2) tail pipe emission against the fresh air flow. The general flow features that develop in this isolated zone (obtained assuming DPM as a

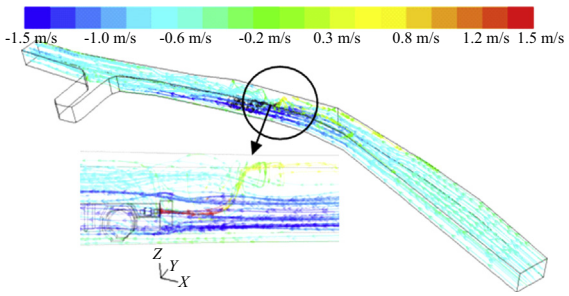


**Fig. 5.** Pathlines colored by $x$-velocity inside the isolated zone at $t$ = 200 s.

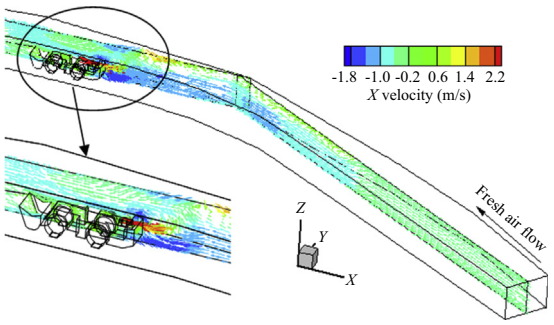


**Fig. 6.** Velocity vectors at a given spanwise plane in the isolated zone at $t$ = 200 s.

particle) is shown using pathlines colored by $x$-velocity in Fig. 5. The emissions from the tailpipe (air and particle streams) start flowing toward the roof of the mine due to the buoyancy force caused by the density difference. This, in turn, is caused by the temperature difference between the fresh intake air and tail pipe emissions forming a turbulent buoyant plume.

This plume then divides into two unequal branches on the roof with some emissions flowing upstream toward the inlet and some flowing downstream toward the exit. A part of the incoming fresh air interacts with tail pipe flow, gets heated up and is pushed upward due to the buoyancy force. The air then reverses flow and starts flowing upstream again. This gives rise to the reversed flow region in the roof area of the mine upstream of LHD. This complex reversed flow region grows in size with time and causes the fresh air flow from the inlet to deflect toward the floor region causing fresh air flow starvation at the upstream ceiling region of the mine. This effect can be clearly seen in Fig. 5. The inlet ventilation rate needs to be increased to avoid this kind of reversed flow behavior in simulation. Similar flow features are obtained assuming species transport approach and hence not shown here due to space limitations.

The velocity vectors colored by streamwise ($x$) velocity obtained from particle modeling approach is shown in Fig. 6 for two dimensional planes that pass approximately through the middle of the computational domain. The complex reversed flow features developing upstream of LHD near the roof of the mine can be clearly seen in Fig. 6. The length of this roof layer or reversed flow region upstream from the LHD depends on the temperature of the exhaust gases, time duration (during which injection from the tailpipe takes place) and on the incoming fresh air flow rate. For a given tailpipe temperature and duration of injection, this upstream roof layer reversed flow region will disappear once the fresh air ventilation is increased beyond critical ventilation flow rate. The determination of this critical ventilation flow rate to avoid this reverse flow condition is beyond the scope of this research paper. The complex flow that develops at the rear side of the LHD due to the interaction between tailpipe emissions, inlet fresh air and the vehicle's solid surface can also be clearly seen in Fig. 6.

The distribution of DPM in the isolated zone is shown in Fig. 7 for both particle tracking and species transport models. Fig. 7a and b shows the DPM distribution for particle tracking model and species transport model. The side view of the isolated zone near LHD is also shown as an inset in Fig. 7a and b. The side view clearly shows the influence of the buoyancy force on the tail pipe emission. The hot diesel exhaust from the tailpipe of LHD starts flowing upwards due to the buoyancy force creating moving roof layer both upstream and downstream from the LHD. During this buoyant motion, DPM will lose heat to the incoming fresh cold air and will get mixed with air (if DPM behaves like as gas) to form a mixture; or will follow the air molecules (if DPM behaves like a sub-micron particle) without mixing due to the Brownian motion of the particles. The comparison of the distribution pattern between the two models clearly shows that DPM, when treated as a gas, diffuses more readily with the air and gets diluted. The roof layer does not have any region far downstream or upstream from the vehicle that has a DPM level beyond the prescribed regulatory limit of 160 $\mu g/m^3$ as shown in Fig. 7b. The high diffusion and mixing between incoming air and DPM (treated as gas) near the tailpipe region (forming a diluted homogenous mixture) results in lower value of DPM concentration. This is not the case for particle model since a higher DPM concentration level (>160 $\mu g/m^3$) occurs on the roof layer both upstream and downstream from LHD. This is due to less diffusion and non-mixing between air and particulate DPM to dilute it near the tailpipe region as shown in Fig. 7a. This non-mixing and less diffusive nature of particle DPM in air results in accumulation of DPM particles on the roof layer compared to the gaseous model which results in high DPM concentration.

This accumulation of DPM particles is not uniform all across the roof layer and some void regions can also be seen at a few locations on the roof layer. The red contoured band regions in the particle DPM distribution show large accumulation of DPM particles in those locations resulting in high DPM concentration. This particle accumulation can be clearly seen in the particle traces colored by particle residence time as shown in Fig. 8. The lack of fresh ventilation air to dilute DPM in the reverse flow regions arising due to the roofing of the exhaust gases upstream of LHD, or to the presence of dead-end areas, or to the presence of LHD vehicle blocking the fresh air flow could cause the DPM concentration to increase.

Although the two models predict different DPM distribution upstream and far downstream from LHD for DPM limit greater than 160 $\mu g/m^3$, the results show that for the important region located around the LHD vehicle, the two models predict approximately similar distribution (not in magnitude) for $DPM_{limit}$ > 160 - $\mu g/m^3$ as can be evidenced from Fig. 7a and b. In this region, miners have to use personal protection instruments and enclosed cabs to protect themselves from the harmful effects of DPM. Some DPM in the roof downstream from LHD cools due to heat transfer between the air and DPM particles causes them to lose upward buoyancy force and, as a result, falling to the floor level as seen in Fig. 7a. This phenomenon is not seen for species transport model outcomes in Fig. 7b for the range of DPM concentration considered for this result.

The purpose of the study is to determine the DPM distribution in the isolated zone and identify any region in that isolated zone that exceeds the DPM threshold limit of 160 $\mu g/m^3$. It should be noted in Fig. 7a and b that the two distributions may differ in magnitude at any given location around the LHD region, but the $DPM_{limit}$ > 160 $\mu g/m^3$ signifies the threshold limit and any concentration above that limit is not acceptable, and hence, from that perspective, the two models predict approximately the same DPM affected zone. If the lower limit of DPM is decreased from 160 to

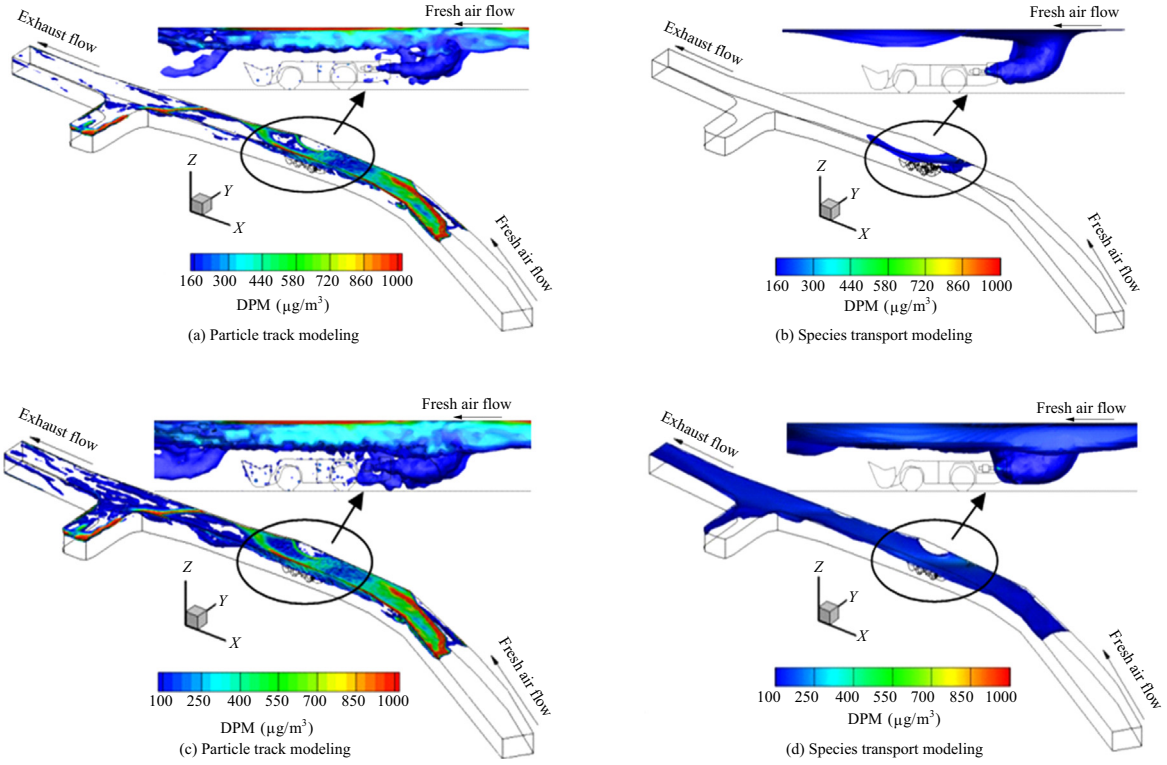


**Fig. 7.** DPM distribution inside the isolated zone at $t$ = 200 s.

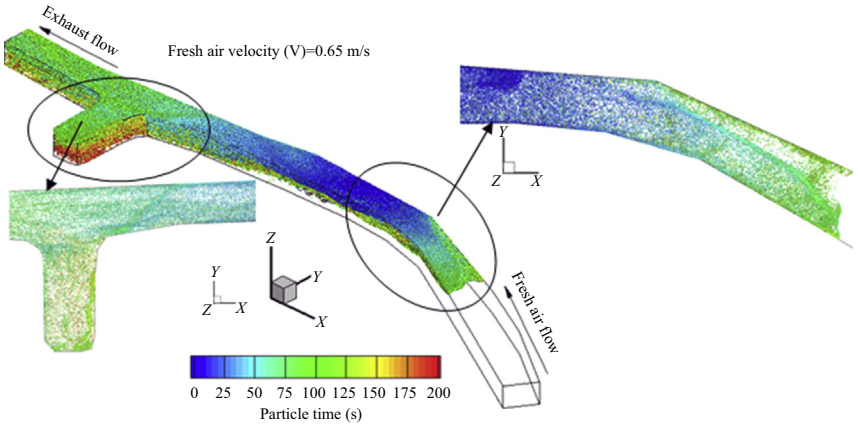


**Fig. 8.** Particle traces colored by particle residence time (s) at $t$ = 200 s.

100 μg/m$^3$, good qualitative agreements between the two distributions can be seen from Fig. 7c and d. It can also be seen that when the lower limit is reduced, the DPM is uniformly distributed for species transport model all along the roof layer compared to particle tracking model.

Fig. 8 shows the DPM residence time inside this single entry and different colors indicate the length of the duration in seconds (residence time) for each particle with red color being the maximum residence time (200 s) and blue being the minimum residence time (0 s). It is obvious from the plots that particle will have minimum residence time at the tail pipe location and maximum residence time at the dead-end entry (the stub entry close to the exit) and at the exit region. The maximum duration for the particle at the dead-end is due to the presence of the air recirculation flow region and any DPM particle caught in that vortex will re-circulate continuously and will rarely escape from that region. The miners working in that dead-end area for a long duration of time may be subjected to higher DPM level values as shown in Fig. 7a. Therefore, adequate protection must be undertaken, such as like auxiliary ventilation fans before venturing to work in those areas. The plan view of the particle residence time distribution in the roof region of the mine is also shown as an inset in Fig. 8 for two locations (1) upstream of LHD and (2) the dead-end region.

The DPM distribution inside the isolated zone at two given spanwise planes is shown in Fig. 9 for both particle tracking and species transport model. Since the isolated zone is not a perfect straight entry but curves from the inlet to the exhaust, two spanwise planes that pass approximately through middle of the single entry were drawn and one of the spanwise planes was also made to pass approximately through the middle of the tailpipe region. The distribution identifies the region of DPM concentration greater than 10 μg/m$^3$. The turbulent plume of the exhaust gases from the

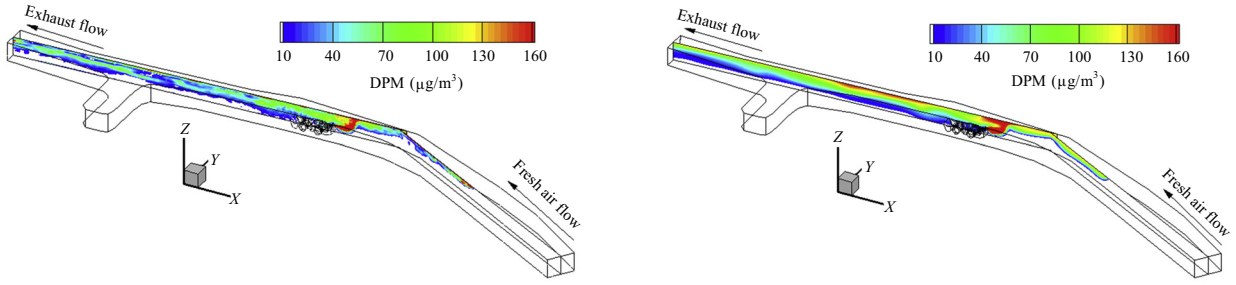


(a) Particle track modeling (b) Species transport modeling

**Fig. 9.** Distribution of DPM inside the isolated zone at a given spanwise plane at $t$ = 200 s.

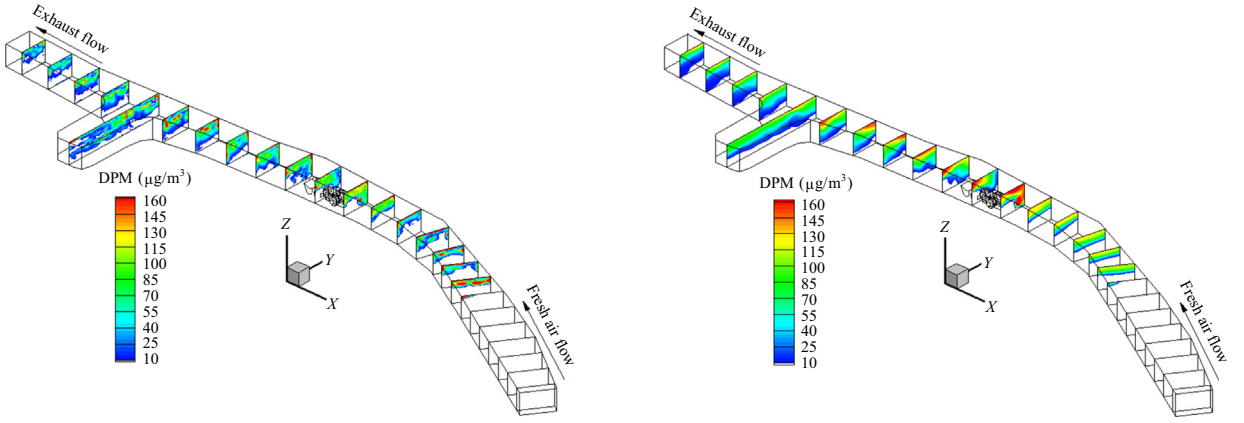


(a) Particle track modeling (b) Species transport modeling

**Fig. 10.** DPM distribution at different cross sectional planes.

tailpipe and the influence of buoyancy force on DPM distribution can be clearly seen from Fig. 9. It can be seen that both of the models give similar DPM affected region although they differ in magnitude. Both the models produce roofing effect upstream of the LHD. Fig. 9 also clearly shows that high concentration DPM (>160 μg/m$^3$) at this spanwise plane appears around the LHD tailpipe region for both the models. However, a few patches of high DPM concentration (>160 μg/m$^3$) occur both upstream and downstream from LHD at the roof region for particle tracking model. The presence of high DPM concentration at the roof level should not hurt the miners as it is not at the breathing level unless for high level working miners, like the manual scaler. The species transport model does not produce DPM concentration higher than the regulatory limit at any locations both upstream and downstream of LHD.

The DPM distribution at different cross sectional planes is shown in Fig. 10a and b respectively. It can be seen again that both models predict qualitatively similar DPM distribution patterns. The red colored region in the distribution shows DPM concentration $\geqslant$160 μg/m$^3$. The plot clearly shows that DPM does not fill all the portion of the cross-sectional planes and are more concentrated toward the roof of the mine due to the buoyancy force caused by the temperature difference. The distribution also shows that the species transport model predicts smooth DPM distribution across the cross sectional planes compared to the particle tracking model. In addition to the region around LHD vehicle, particle tracking model results show that high concentration DPM exists both upstream and downstream of LHD as small patchy areas and are mostly located at the roof or near the roof areas throughout the isolated zone. The species transport model does not show such distribution due to the thorough mixing and dilution it undergoes with air. The only location where high concentration DPM is present is around LHD areas for the species transport model. The particle tracking model also shows high DPM concentration areas inside the dead-end at the roof region whereas species transport model shows those regions are well diluted below the permissible limits.

The comparison of particle and species modeling approaches is also made by comparing area weighted average DPM values at different cross-sectional planes as shown in Fig. 11a. The cross-sectional planes inside the single entry are shown in green color in Fig. 11b. There is an excellent agreement between the two models, although discrete phase modeling tends to over predict the DPM concentration upstream and under predict it downstream from the LHD. The discrepancy between the two models at the upstream location is due to the accumulation of DPM particles on the roof layer in the particle tracking approach. The result is high DPM concentrations as explained in the previous section. This accumulation also results in extending the length of the roofing layer upstream of LHD by approximately 5 m for the particle tracking model when compared with the species transport model and can be seen clearly in Figs. 10 and 11a. In other words, the DPM unaffected region is 5 m longer for species transport results compared to particle tracking results. This high concentration of averaged DPM upstream of LHD requires low concentration of averaged DPM downstream from LHD to satisfy the mass conservation. Fig. 11 also shows that maximum averaged DPM occurs at the tailpipe location as expected. It drops suddenly from this peak value and achieves a local minimum value at the bucket region of the LHD. Thereafter, averaged DPM reaches an approximately constant value before it encounters the dead-end area located at the downstream region to attain a local maximum. At the first plane of the three cross sectional planes inside the dead-end area shown in

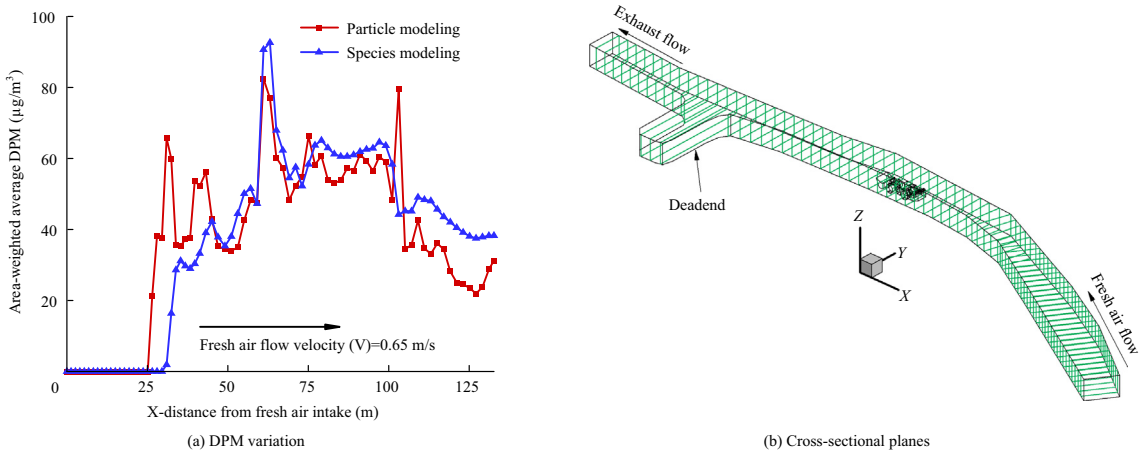


(a) DPM variation (b) Cross-sectional planes

**Fig. 11.** Comparison of averaged DPM values at different streamwise planes using particle and species model at $t$ = 200 s.

Fig. 11b, particle model predicts very high averaged DPM concentration due to the accumulation of DPM particles at the left roof corner of the dead-end as shown in Fig. 8. The species model shows a drop in the averaged DPM concentration for that location. This is due to the increase in the cross sectional area for the dead-end planes and the fact that DPM is already well diluted to be distributed smoothly for most of the upper section of that cross-sectional plane as shown in Fig. 10b.

## 7. Conclusions

Three dimensional simulations of DPM emission and its distribution pattern are studied using Ansys Fluent CFD code for the portion of an isolated zone used for DEEP field study. The DPM is released from the LHD vehicle operating inside the isolated zone with its tail pipe emission against the direction of the fresh air flow.

Both species transport model and particle tracking model available in Fluent were used for the DPM simulation. In the particle tracking model, DPM was assumed to behave like a particle; and in the species transport model, DPM was assumed to behave like gas. Numerical simulation shows that a strong buoyancy force develops due to large temperature differences between the tail pipe and inlet fresh air temperature. This buoyancy force causes the non-uniform DPM distribution across the cross sections inside the single entry and seems to be strongly localized near the ceiling. The simulation results show that both models can be used to predict DPM distribution pattern inside the isolated zone.

Some difference in the distribution pattern inside the mine may arise depending on the choice of treatment of DPM as a gas or as a particle. This difference is due to the ease with which DPM, as a gas, can diffuse and mix readily with air as opposed to DPM as a particle.

However, the comparison between the DPM contours around the important region surrounding the LHD areas shows that both the models produce similar distribution patterns and can successfully identify the regions with high DPM concentrations. The comparison between the two models for the area weighted average DPM values at different cross sectional planes inside the isolated entry shows very good agreement and further emphasizes the fact that both models can be used for successful DPM distribution determination inside the isolated zone.

The results show that the computational time and memory space requirements reduce when DPM is treated as gas and increase when DPM is treated as particle. This computational time and memory space requirements for DPM (as particle) will increase manifold and may become unmanageable with multiple mining operations, dynamic operating systems, auxiliary ventilation systems, and complex underground mine design layout. Since the present study shows that both models can be used for DPM determination, the species transport model will be an ideal choice to study the DPM distribution pattern inside the underground mine due to the economic reasons outlined above.

## Acknowledgments

The authors wish to express their sincere gratitude to the financial support provided by the Western US Mining Safety and Health Training & Translation Center by the National Institute for Occupational Safety and Health (NIOSH).

## References

[1] NIOSH. Carcinogenic effects of exposure to diesel exhaust. National Institute for Occupational Safety and Health (NIOSH). Department of Health & Human Services; 1988.
[2] EPA. Health assessment document for diesel engine exhaust. U.S. Environmental Protection Agency; 2002.
[3] ACGIH. Threshold limit values for chemical substances and physical agents and biological exposure indices. Cincinnati: American Conference of Governmental Industrial Hygienists; 2013.
[4] Kahn G, Orris P. Acute overexposure to diesel exhaust: report of 13 cases. Am J Ind Med 1988;13(3):405–6.
[5] Rundell B, Ledin MC, Hammarstrom U, Stjernberg N, Lundback B, Sandstrom T. Effects on symptoms and lung function in humans experimentally exposed to diesel exhaust. Occup Environ Med 1996;53(10):658–62.
[6] Wade III JF, Newman LS. Diesel asthma: reactive airways disease following overexposure to locomotive exhaust. J Occup Med 1993;35(2):149–54.
[7] Kim D, Gautama M, Gerac D. Parametric studies on the formation of diesel particulate matter via nucleation and coagulation modes. J Aerosol Sci 2002;33(12):1609–21.
[8] Uhrnera U, Von Lowis S, Vehkamaki H, Wehner B, Brasel S, Hermann M, Stratmann FM, Kulmala M, Wiedensohler A. Dilution and aerosol dynamics within a diesel car exhaust plume-CFD simulations of on-road measurement conditions. Atmos Environ 2007;41(35):7440–61.
[9] Desantes JM, Margot X, Gil A, Fuentes E. Computational study on the deposition of ultrafine particles from Diesel exhaust aerosol. J Aerolsol Sci 2006;37(12):1750–69.
[10] Ström H, Andersson B. Simulations of trapping of diesel and gasoline particulate matter in flow-through devices. Top Catal 2009;52(13):2047–51.
[11] Ray RE, Kang K, Gilbey M. CFD analysis of diesel emission in a railroad tunnel. In: Proceeding of the 10th U.S./North American mine ventilation symposium. Alaska, USA; 2004. p. 117–26.
[12] Zheng Y, Tien JC. DPM dispersion study using CFD for underground metal/non-metal mines. In: Proceeding of 12th U.S./North American mine ventilation symposium. USA: University of Nevada Reno, Nevada; 2008. p. 487–93.
[13] Zheng Y, Thiruvengadam M, Lan H, Tien JC. Simulation of DPM distribution in a long single entry with buoyancy effect. Int J Min Sci Technol 2015;25(1):47–52.
[14] Zheng Y, Lan H, Thiruvengadam M, Tien JC. DPM dissipation experiment at MST's experimental mine and comparison with CFD simulation. J Coal Sci Eng 2011;17(3):285–9.

[15] Kurnia CJ, Sasmito PA, Wong YW, Mujumdar SA. Prediction and innovative control strategies for oxygen and hazardous gases from diesel emission in underground mines. Sci Total Environ 2014;481:317–34.
[16] Yuan L, Smith AC. Computational fluid dynamics modeling of spontaneous heating in longwall gob areas. Trans Soc Min Metall Explor 2007;322:37–44.
[17] Ren TX, Balusu R. The use of CFD modeling as a tool for solving mining health and safety problems. In: Proceedings of 10th underground coal operators' conference. Brisbane, QLD, AU; 2010. p. 339–49.
[18] Zhou L, Pritchard C, Zheng Y. CFD modeling of the methane distribution at a continuous miner face with various curtain setback distances. Int J Min Sci Technol 2015;25(4):635–40.
[19] Hargreaves DM, Lowndes IS. The computational modeling of the ventilation flows within a rapid development drivage. Tunn Undergr Space Technol 2007;22(2):150–60.
[20] Wala AM, Vytla S, Huang G, Taylor CD. Mine face ventilation: a comparison against bench-mark experiments for the CFD code validation. Min Eng 2007;59(10):49–55.
[21] Kollipara VK, Chugh YP, Relangi DD. A CFD analysis of airflow patterns in face area for continuous miner making a right turn cut. In: Proceedings of the SME annual meeting. Seattle, WA, USA; 2012. p. 12–132.
[22] Torno S, Toraño J, Ulecia M, Allende C. Conventional and numerical models of blasting gas behavior in auxiliary ventilation of mining headings. Tunn Undergr Space Technol 2013;34:73–81.
[23] Ren TX, Balusu R. Innovative CFD modeling to improve dust control in longwalls. In: Proceedings of coal operators' conference. Wollongong, NSW, AU; 2008. p. 137–42.
[24] Ren TX, Wang Z, Cooper G. CFD modelling of ventilation and dust flow behavior above an underground bin and the design of an innovative dust mitigation system. Tunn Undergr Space Technol 2014;41:241–54.
[25] Xu G, Luxbacher KD, Ragab S, Schafrik S. Development of a remote analysis method for underground ventilation systems using tracer gas and CFD in a simplified laboratory apparatus. Tunn Undergr Space Technol 2013;33:1–11.
[26] McGinn S, Grenier M, Gangal M, Rubeli B, Bugarski A, Schnakenberg G, et al. Diesel emissions evaluation program (DEEP) final report of investigation; 2004.
[27] Messerer A, Niessner R, Poschl U. Thermophoretic deposition of soot aerosol particles under experimental conditions relevant for modern diesel engine exhausts gas systems. J Aerosol Sci 2003;34:1009–21.
[28] Anon.. Ansys Fluent 12.0 user's guide. ANSYS Inc.; 2013.
[29] Zheng Y, Thiruvengadam M, Lan H, Tien JC. Simulation of DPM distribution in a long single entry. In: Proceedings of 13th U.S./North American mine ventilation symposium. Sudbury, Ontario, Canada; 2010. p. 149–56.
[30] Zheng Y, Thiruvengadam M, Lan H, Tien JC. Effect of auxiliary ventilations on diesel particulate matter dispersion inside a dead-end entry. Int J Min Sci Technol 2015;25(6):927–32.